Formins specify membrane patterns generated by propagating actin waves

Mary Ecke[a], Jana Prassler[a], Patrick Tanribil[a], Annette Müller-Taubenberger[b], Sarah Körber[c], Jan Faix[c,*], and Günther Gerisch[a,*]

[a]Max Planck Institute of Biochemistry, D-82152 Martinsried, Munich, Germany; [b]Department of Cell Biology (Anatomy III), Ludwig Maximilian University of Munich, D-82152 Planegg-Martinsried, Munich, Germany; [c]Institute of Biophysical Chemistry, Hannover Medical School, D-30625 Hannover, Germany

ABSTRACT **Circular actin waves separate two distinct areas on the substrate-attached cell surface from each other: an external area from an inner territory that is circumscribed by the wave. These areas differ in composition of actin-associated proteins and of phosphoinositides in the membrane. At the propagating wave, one area is converted into the other. By photo-conversion of Eos-actin and analysis of actin network structures we show that both in the inner territory and the external area the actin network is subject to continuous turnover. To address the question of whether areas in the wave pattern are specified by particular actin polymerizing machines, we locate five members of the formin family to specific regions of the wave landscape using TIRF microscopy and constitutively active formin constructs tagged with fluorescent protein. Formin ForB favors the actin wave and ForG the inner territory, whereas ForA, ForE, and ForH are more strongly recruited to the external area. Fluctuations of membrane binding peculiar to ForB indicate transient states in the specification of membrane domains before differentiation into ForB decorated and depleted ones. Annihilation of the patterns by 1 μM of the formin inhibitor SMIFH2 supports the implication of formins in their generation.**

Monitoring Editor
Leah Edelstein-Keshet
University of British Columbia

Received: Aug 21, 2019
Revised: Jan 7, 2020
Accepted: Jan 8, 2020

INTRODUCTION

Wave patterns on the substrate-attached surface of *Dictyostelium* cells provide a system in which two different states of actin organization are continuously interconverted. The sites of interconversion are propagating actin waves that circumscribe an inner territory, the organization of which is distinct from that of the external area, the region outside of the closed circular wave (Schroth-Diez *et al.*, 2009). The phosphatidyl-inositol (3,4,5)-trisphosphate (PIP3)-rich state of the inner territory has a limited lifetime (Gerhardt *et al.*, 2014). Its conversion to the external area is accompanied by the insertion of a trailing wave, which typically propagates at a distance behind a leading wave. Whereas a leading wave propagates toward the external area, in that way increasing the size of an inner territory, a trailing wave propagates into internal territory thus decreasing its size. We also used the term "retracting wave" for a trailing wave (Gerisch *et al.*, 2011).

For imaging, the wave patterns have the advantage to develop on a planar substrate surface, which renders them easily accessible to total internal reflection (TIRF) and confocal fluorescence microscopy. Large cells generated by electric pulse–induced fusion provide sufficient space for the actin waves to propagate, to fuse, and to retract (Gerisch *et al.*, 2013; Gerhardt *et al.*, 2014).

In the actin wave patterns, changes in membrane phosphoinositide composition and Ras activation (Fukushima *et al.*, 2019) are coupled to changes in the prevalence of actin-associated proteins (Gerisch *et al.*, 2011). The inner territory resembles the front region of a polarized motile cell in its high PIP3 content and enrichment in the Arp2/3 complex, whereas the external area resembles in

This article was published online ahead of print in MBoC in Press (http://www.molbiolcell.org/cgi/doi/10.1091/mbc.E19-08-0460) on January 15, 2020.

Author contributions: G.G. designed the project and wrote the paper; M.E., J.P., and P.T. conducted the experiments and analyzed the data; A.M.T. created the DdEos-actin vector; S.K. and J.F. designed the formin constructs.

The authors declare no competing or financial interests.

*Address correspondence to: Günther Gerisch (gerisch@biochem.mpg.de); Jan Faix (faix.jan@mh-hannover.de).

Abbreviations used: DAD, diaphanous autoregulatory domain; DID, diaphanous inhibitory domain; PB, phosphate buffer; PIP3, phosphatidyl-inositol (3,4,5)-trisphosphate; sf, superfolder; SRRF, superresolution radial fluctuation; TIRF, total internal reflection fluorescence.

the abundance of myosin-II filaments and accumulation of the actin-bundling protein cortexillin the contractile tail of the cell (Schroth-Diez *et al.*, 2009; Gerisch *et al.*, 2012). The wave pattern is also comparable to a frustrated phagocytic cup spreading on a planar surface, with the actin wave corresponding to the border and the inner territory to the basal area of an incipient cup (Gerisch *et al.*, 2009).

Previous work based on FRAP indicated that the waves propagate by actin polymerization at their front rather than by net transport of actin filaments (Bretschneider *et al.*, 2009). The actin architecture visualized by cryo-electron tomography revealed no preferential orientation of actin filaments in the direction of wave propagation, suggesting that the waves propagate by de novo nucleation of actin filaments beneath the plasma membrane (Jasnin *et al.*, 2019). The cryo-electron tomograms also revealed that the external area, actin wave, and inner territory are distinguished by the architecture of their actin networks.

In the present work, we show that the actin network in the inner territory as well as in the external area is under continuous renewal, suggesting the ubiquitous presence of factors that drive actin polymerization, thereby maintaining the architecture of each area. The continuous turnover of filamentous actin at all sites of the wave pattern raised the question of which proteins are responsible for the nucleation and elongation of actin filaments at these different sites. When cells are cultivated on perforated membranes, they form protrusions into the holes at the sites of actin waves. This capacity is abrogated by the small molecule formin inhibitor SMIFH2, suggesting that formins are essential for actin-based activities in waves (Jasnin *et al.*, 2016). Cells of *Dictyostelium discoideum* express 10 different formins, ForA to ForJ; six of them are strongly expressed during growth and at early stages of development when actin waves are formed (Rivero *et al.*, 2005).

According to previous reports, the formins studied are recruited to different sites in a migrating or phagocytosing cell. ForA is functionally related to vertebrate mDia1; it localizes to the trailing edge of migrating *Dictyostelium* cells where it stabilizes the actin cortex, thus preventing blebbing on actomyosin contraction in 2D-confinement (Ramalingam *et al.*, 2015). This localization of ForA to the rear of the cells depends on both its PI(4,5)P2-binding C2 domain and a GTPase-binding site in its N-terminal region. ForA collaborates with ForH (= dDia2) and ForE (= dDia3) to safeguard integrity of the contractile actin cortex. Triple mutant cells devoid of these formins are not able to migrate in 2D-confinement under a thin sheet of agar, and they have massive defects in cortical rigidity, cytokinesis, as well as in development (Litschko *et al.*, 2019). The constitutively active variants of ForE and ForH localize to the cell cortex, and they accumulate most prominently at the tips of filopodia (Schirenbeck *et al.*, 2005; Litschko *et al.*, 2019).

ForB is mainly expressed in the growth phase and early development (Rivero *et al.*, 2005); its function remains to be characterized (Kitayama and Uyeda, 2003).

ForG is highly enriched in phagocytic and macropinocytic cups and is involved in the assembly of actin at the base of the cups (Junemann *et al.*, 2016). Accordingly, ForG is required for efficient particle and bulk fluid uptake. For appropriate targeting of ForG, its interactions with activated RasB or RasG, and likely with PIP3, are important. ForG has only a weak actin-filament nucleating activity in vitro but considerably promotes elongation. Therefore, ForG has been suggested to cooperate with the Arp2/3 complex in elongating filaments in a branched actin network (Junemann *et al.*, 2016).

Active ForF (= dDia1) populates the entire pseudopod except for the very tip region adjacent to the membrane and is required for efficient phototaxis and formation of properly sized fruiting bodies (Winterhoff *et al.*, 2014).

Here we explore the diverse distributions of these formins to specific sites in the wave landscape and the dynamics of their redistribution during wave propagation. For comparison, we show that the actin assembly factor VASP distributes throughout all regions of the wave pattern, rendering it unlikely that VASP is responsible for regional differences in actin organization. Only a single VASP is encoded in the genome of *D. discoideum* (Han *et al.*, 2002), in contrast to the presence of multiple formins. The formins studied are members of the Diaphanous-related subfamily that exist in an autoinhibited basal state (Watanabe *et al.*, 1999; Alberts, 2001) that is maintained by interaction of the C-terminal DAD (diaphanous autoregulatory) domain with the N-terminal DID (diaphanous inhibitory) domain (Lammers *et al.*, 2005; Nezami *et al.*, 2006; reviewed by Goode and Eck, 2007). The inhibition can be partially relieved by binding of a Rho-GTPase to an N-terminal site extending from a GTPase-binding domain to the DID (Li and Higgs, 2005). In addition, other factors contribute to membrane localization, as shown for mammalian Dia1 (Seth *et al.*, 2006). This formin binds to PI(4,5)P2, which, however, inhibits rather than promotes the actin polymerization activity (Ramalingam *et al.*, 2010). To avoid the background of diffusively distributed full-length formins, constitutively active constructs lacking the DAD are being used as, for instance, by Seth *et al.* (2006) for mouse Dia1 and FRLα, and by Litschko *et al.* (2019) for *Dictyostelium* formins A, E, and H.

Assigning activated formins ForA, ForG, and ForB, respectively, to the external area, the inner territory, and the actin wave, implies that formins are present in all regions of the wave pattern. High sensitivity of wave formation to the formin inhibitor SMIFH2 indicates a pivotal role of formins in generating the pattern. Using the formins as indicators, we explore mechanisms of pattern generation with a focus on ForB fluctuations to unveil transitory states in pattern development.

RESULTS

Dynamics of actin networks at different sites of the wave pattern

To illustrate the patterns generated by actin waves beneath the substrate-attached membrane of *D. discoideum* cells, a large cell forming multiple waves is depicted in Figure 1A. Enrichment in the phosphoinositide PIP3 distinguishes the membrane of the inner territories, each surrounded by a circular wave, from that of the external area. The actin waves represent transition zones of actin structures in the cell cortex: at the site of an expanding wave, the loose actin network of the external area is converted into the dense fabric of the inner territory (Bretschneider *et al.*, 2009; Jasnin *et al.*, 2019). This could imply that the network structures in the external area and the inner territory are stationary, such that remodeling is restricted to the propagating wave. Alternatively, the actin structures at all sites of the pattern may be short lived and under continuous renewal. To distinguish between these possibilities, we employed photoconversion of Eos-actin to determine actin turnover in the inner territory. In the external area, the network of actin filaments proved to be too loose for photoconversion to produce appropriate signals against the cytoplasmic background of G-actin. In this area we used decoration with ABP120, the filamin orthologue of *Dictyostelium*, to analyze the network of bundled actin filaments.

Eos-actin was converted to the red fluorescent state by illuminating a spot in the external area at 405 nm. Since photoconversion was accomplished by a focused light beam in bright-field rather

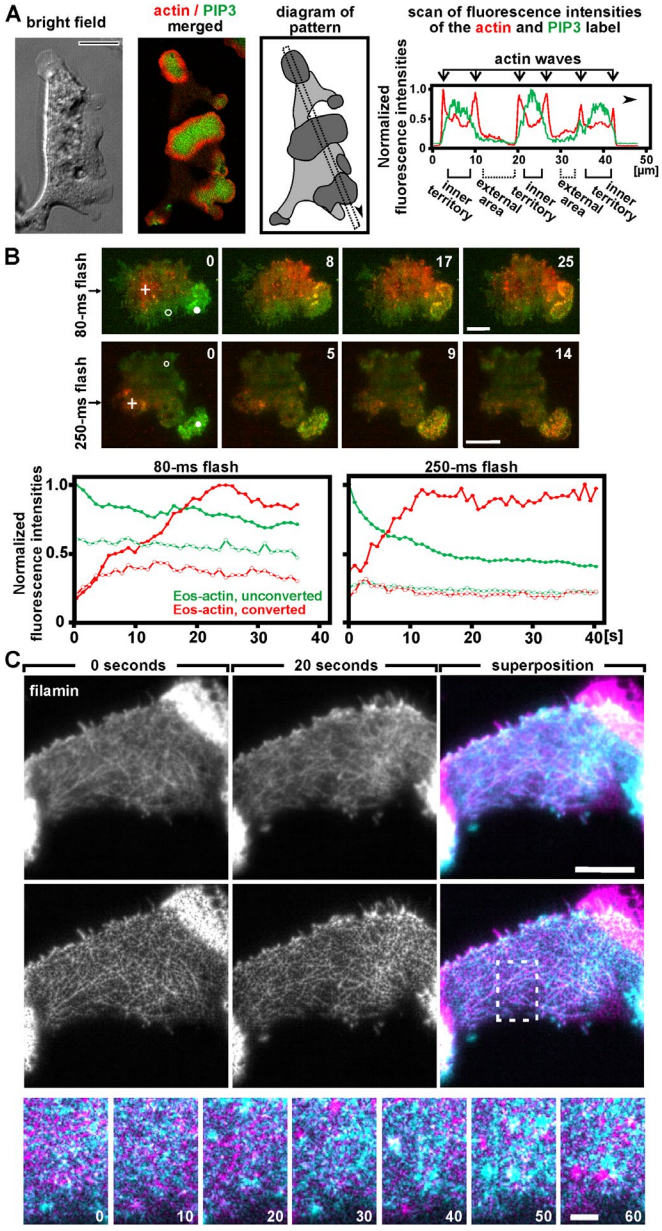

FIGURE 1: Actin wave patterns and their dynamics at the substrate-attached surface of *D. discoideum* cells. (A) A large cell produced by electric pulse–induced fusion expressing mRFP-LimEΔ as a label for filamentous actin (red) and GFP-PHcrac for PIP3 (green). From left to right: DIC-brightfield image of the cell, merged TIRF image, diagram displaying the inner territories in dark and the external areas in light gray, and scan of fluorescence intensities along the line indicated in the diagram. Bar, 10 µm. (B) Actin turnover in the inner territory revealed by the incorporation of photoconverted Eos-actin. Top panels: two time series of fluorescence images of the converted red form of Eos-actin and the unconverted green form in large cells. For the time series on top an 80-ms flash, for that on bottom a 250-ms flash from a 405-nm laser was applied. Merged TIRF images of unconverted Eos-actin (green) and of the photoconverted one (red) are displayed. The single-channel images are shown as Supplemental Figure S1. Crosses indicate the centers of the flashes; closed circles indicate the positions of fluorescence recording in an inner territory; open circles indicate the positions of reference recording in an external area. Time is indicated in seconds after the first frame. Bars, 10 µm. Bottom panels: scans of the temporal changes in fluorescence intensities of the unconverted (green) and the converted (red) Eos-actin; closed and open circles correspond to the recording positions in the images on top. In each panel, the curves are normalized to the highest value in either the green or the red channel. The 0-s frames were acquired in the left panels at 1.0 s and in the right panels at 1.9 s after the converting flash. (C) Network dynamics in the external area visualized by GFP-filamin. Top panels: TIRF images showing a large cell with an expanded external area where filamin-decorated network structures are seen. Two internal territories at the borders of the frame show dense packing of the filamin. The same area is displayed at two time points separated by 20 s and with color-coded overlay of the 0-s (magenta) and 20-s (cyan) images. Bar, 10 µm. Middle panels: the images shown in the top panels after reconstruction through the SRRF algorithm. The full sequence is shown in Supplemental Video S1. Bottom panels: details of the area framed in the reconstructed merged image are shown enlarged and at higher temporal resolution. Each panel represents gains (cyan) and losses (magenta) of fluorescence intensity recorded at 1-s intervals and summed up for a period of 10 s. Bar, 2 µm.

than in the TIRF mode, primarily diffusible G-actin in the cytoplasm became converted. Incorporation of the converted actin into cortical structures of the inner territory was then imaged by TIRF microscopy. Figure 1B shows two recordings that differ in the length of the converting flash at 405 nm: 80 and 250 ms, the latter supposed to result in a higher rate of green-to-red converted actin. The half times of incorporation were 12 s for the 80-ms flash and 6 s for the 250-ms flash. These numbers are upper limits since, for technical reasons, there was a delay of 1.0 s for the 80-ms flash and of 1.9 s for the 250-ms flash between conversion and acquisition of the first image. The incorporation into new actin filaments in the 10-s range provides proof for the continuous polymerization activity in the inner territory.

To visualize actin reshuffling in the external area, we used GFP-tagged filamin (ABP120) as an actin-binding protein that decorates the loose network of actin bundles, which are characteristic of this area as revealed by cryo-electron tomography (Jasnin *et al.*, 2019). The images in the top panels of Figure 1C show changes in network structure within an interval of 20 s, indicating by color-coding the changes of fluorescence intensities in the two frames. The middle panels and Supplemental Video S1 show the same structures after processing through the SRRF (super-resolution radial fluctuation) algorithm (Gustafsson *et al.*, 2016; Culley *et al.*, 2018; Laine *et al.*, 2019). The nonoverlapping structures provide evidence for the continuous shape changes of the network.

The bottom panels in Figure 1C illustrate the gains and losses of fluorescence intensity at the temporal resolution of 1 s, each panel representing the sum of changes during one 10-s interval. These data indicate reorganization on the scale of seconds, in accord with the dynamics of actin bundles on the substrate-attached cell surface in the absence of wave formation, where actin polymerization was analyzed on the subsecond scale (Diez *et al.*, 2005).

Together, the photoconversion of Eos-actin, FRAP applied to actin waves (Bretschneider *et al.*, 2009), and actin network decoration with filamin, indicate that the actin network is continuously remodeled at all sites of wave patterns, suggesting that at each site proteins promoting actin polymerization are required.

Ubiquitous presence of VASP and specific locations of formins in wave patterns

We localized VASP, a major elongation factor of actin filaments in *Dictyostelium* (Breitsprecher *et al.*, 2008), in the wave patterns by dual fluorescence imaging of cells that expressed GFP-VASP (Schirenbeck *et al.*, 2006; Breitsprecher *et al.*, 2008) together with the F-actin probe mRFP-LimEΔ (Bretschneider *et al.*, 2004;

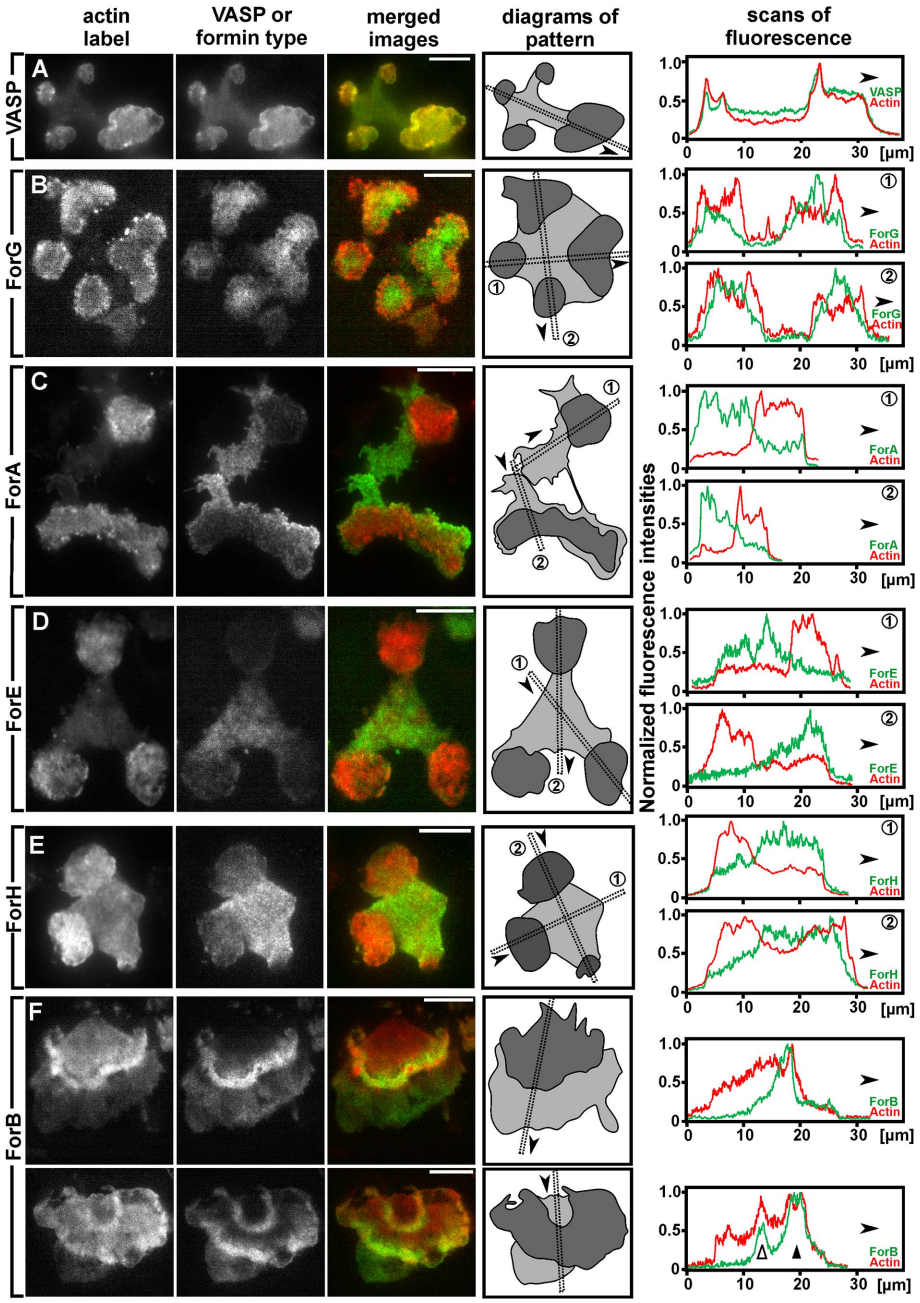

FIGURE 2: Overview of the localization of VASP and of five different formins in actin wave patterns. Large cells of *D. discoideum* produced by electric pulse–induced fusion-expressed fluorescent VASP or one formin construct, together with mRFP-LimEΔ as a reference for F-actin. The merged TIRF images display VASP or the formin construct in green and the actin label in red. Bars, 10 µm. The diagrams indicate the inner territories in dark and the external areas in light gray. Directions of the scans of fluorescence intensity are indicated in the diagrams. The scans in the right panels display in red the fluorescence intensities of the actin label and in green those of GFP-VASP or the formin construct. The intensities are normalized by setting the highest value of each scan to 1. (A) A cell expressing GFP-VASP (full length). (B) A cell expressing YFP-ForG-N. This cell forms four circular waves on its substrate-attached surface, with the ForG construct strongly enriched in the inner territories. (C) An irregularly shaped cell expressing GFP-ForAΔDAD, which is depleted in the inner territories. (D) A cell expressing GFP-ForE-N. This cell forms three waves showing the inner territories depleted of the ForE construct similar to ForA. (E) A cell expressing GFP-ForH-ΔDAD, which is depleted in the inner territories, similar to the ForA and ForE constructs. (F) Two cells expressing GFP-ForBΔDAD showing the ForB construct enriched in the actin waves. The cell on top forms one wave separating the outer area from the inner territory distinguished by its enrichment in actin. The cell on bottom forms a leading and a trailing wave, both enriched in ForB. In the scan on the right, the trailing wave is indicated by an open arrowhead and the leading wave by a closed one.

Fischer *et al.*, 2004). VASP was distributed throughout all parts of the pattern, with minor differences relative to the actin label (Figure 2A).

According to these and previous data (Figure 5 in Jasnin *et al.*, 2019), VASP contributes to the generation of actin filaments in the wave-generating system, but due to its ubiquitous presence it is hardly responsible for differences in the actin architecture of the external area and inner territory. Therefore, in the following, we focus on formins, exploiting their specific distributions in detail. Again, large cells produced by electric pulse–induced fusion were used, in which the waves have sufficient space to travel over long distances and to interact with each other. To determine the different localizations of six formins in the wave pattern, GFP- or YFP-tagged constitutively active formin constructs lacking the autoinhibitory DAD domain were expressed together with the F-actin probe as a reference. The constructs of ForE and ForG comprised an N-terminal fragment (ForE-N and ForG-N, respectively) that prevents excessive actin polymerization. ForG-N has been shown to localize as the ΔDAD construct does (Junemann *et al.*, 2016).

ForF turned out to be present at the entire substrate-attached cell surface; since it did not show a clear preference for specific sites in the pattern, this formin was not pursued further. The distributions of the other five formins in wave patterns are compiled in Figure 2, B–F. ForG localized to inner territories, ForA, ForE, and ForH preferentially to the external area, and ForB was most strongly enriched in the waves. The distinct localizations of these formins enabled us to use them as markers for the study of pattern dynamics during propagation of the waves and during their fusion and splitting.

ForG is targeted to the inner territories

The N-terminal ForG construct employed, YFP-ForG-N, is unable to polymerize actin owing to the absence of the FH2-domain, but it is capable of binding to RasB and RasG, its target sites at the membrane (Junemann *et al.*, 2016). Wave dynamics in the large cells shown in Figure 3A and in Supplemental Video S2 illustrate the reversible association of ForG-N with inner territories at all stages of their expansion or retraction, during their fusion and partition. Figure 3A also underscores the instability of inner territories after exceeding a certain size, as outlined previously (Gerhardt *et al.*, 2014). When the entire substrate-attached area of the large cell was decorated with ForG-N,

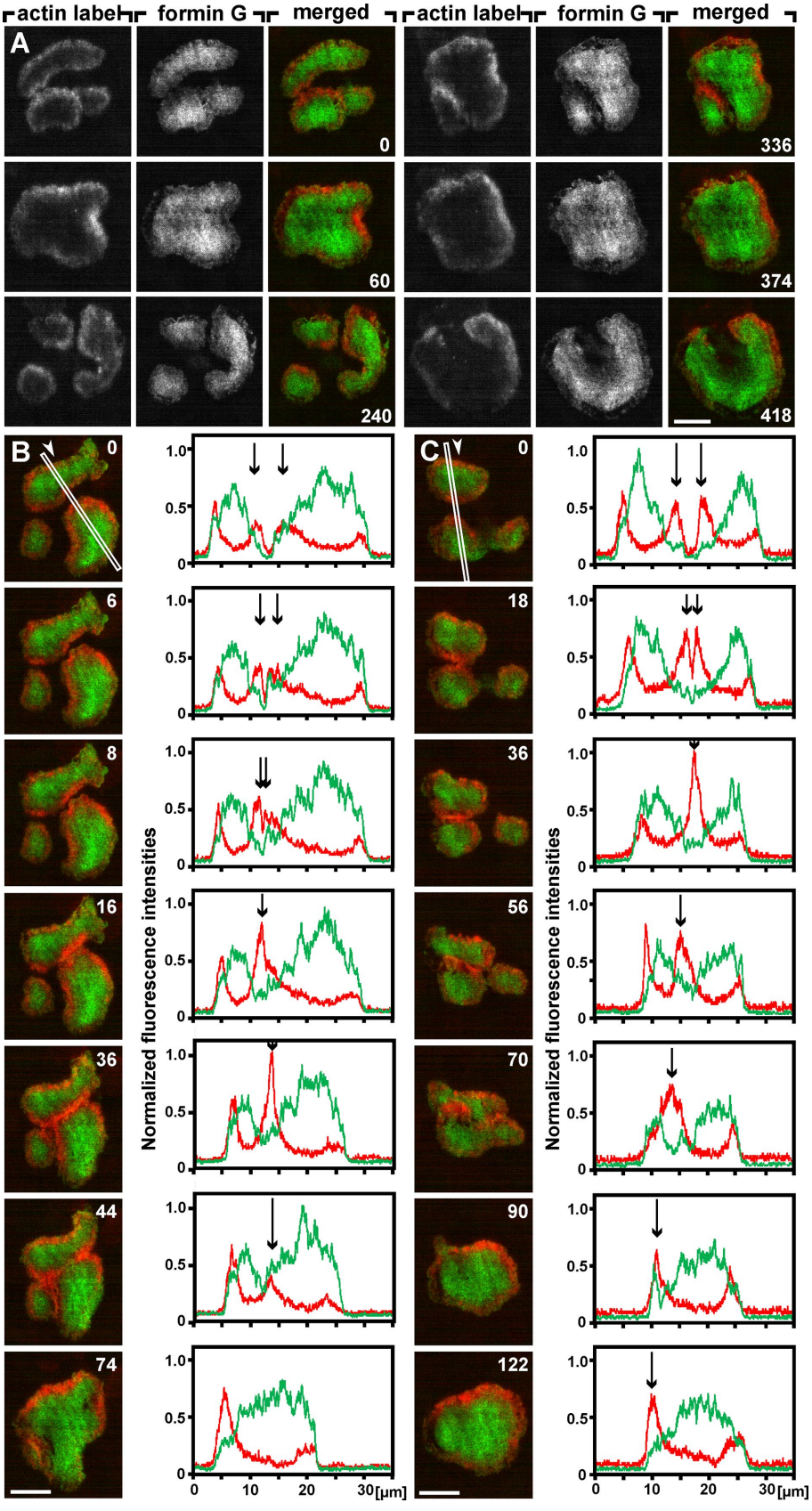

FIGURE 3: ForG dynamics in accord with wave propagation, visualized in TIRF images of large cells. The cells expressed YFP-ForG-N, together with mRFP-LimEΔ as a reference for filamentous actin. In the merged images and in the scans, YFP-ForG-N is shown in green and the actin label in red. Times in the images are indicated in seconds after the first frame of each series. Bars, 10 µm. (A) Time series showing the fusion and splitting of inner territories and finally the formation of a U-shaped configuration characteristic of wave patterns (Gerhardt *et al.*, 2014). All these changes are accompanied by the redistribution of ForG to the inner territory. (B) Two actin waves that collide (0- to 16-s frames), fuse (36-s frame) and eventually extinguish each other followed by the reassembly of ForG in the middle of the scanned line (44- and 74-s frames). Another recording of mutual wave extinction is shown in Supplemental Video S3. (C) Of two propagating actin waves that join each other (0-s to 36-s frames), one wave continues to propagate (56-s to 122-s frames). A similar case is shown in Supplemental Video S4. In B and C, the TIRF images are displayed on the left and corresponding scans of fluorescence intensities on the right. Scan directions are shown in the first images. Arrows in the scans indicate peak positions of the actin waves.

part of the area became depleted of the formin construct (240-s frame in Figure 3A), often resulting in a U-shaped pattern of decoration (374- to 418-s frames). Subsequently, the ForG-N decorated areas expanded again, until they fused while the surrounding actin waves extinguished each other.

Within the inner territories, ForG-N formed mobile micropatches (Supplemental Video S2). At the border of these territories, the labeling with ForG-N declined, such that the encircling wave, intensely labeled for actin, was only weakly decorated with the ForG construct. Nevertheless, there were delicate and highly dynamic ForG structures in these wave areas. In particular, at sites of rapid wave expansion, a margin of ForG-N decorated the wave front (Figure 3A, 240-s frame).

Upon the collision of actin waves, one may proceed

Since the large cells used generate multiple waves, they are suitable to study ForG dynamics during the interaction of waves on sites of collision. Figure 3, B and C, illustrate two cases of propagating actin waves that collide with each other. In each case, the waves propagate into the external area, converting it into strongly ForG decorated inner territory. In Figure 3B, the waves extinguish each other on collision, the area between the waves acquiring full ForG decoration on disappearance of the merged wave (74-s frame). A similar example is shown in Supplemental Video S3.

The extinction of colliding actin waves is in accord with the notion that the wave represents an excited state and is followed by a refractory phase. In fact, we did not observe two waves that crossed each other. However,

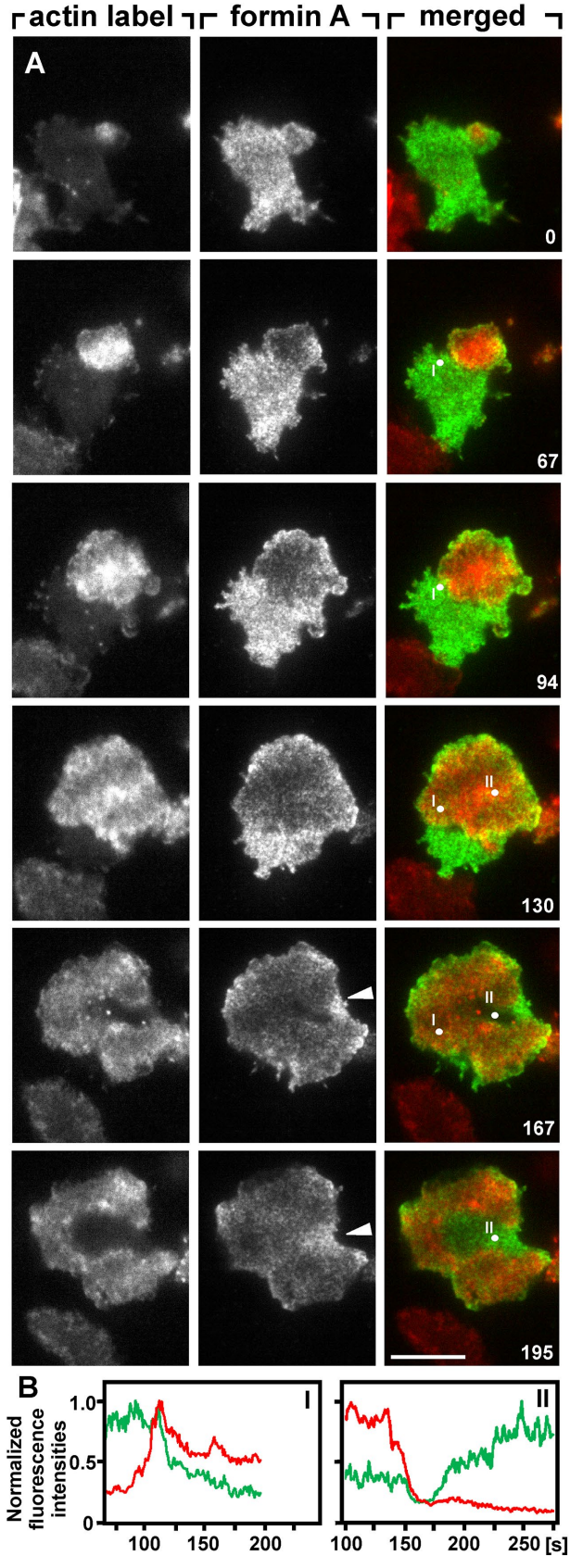

FIGURE 4: ForA dynamics in relation to an expanding and a retracting actin wave. (A) Time series showing TIRF images of the mRFP-LimEΔ label for filamentous actin and of GFP-ForAΔDAD. The merged images show the actin label in red and ForA in green. The same sequence is shown in Supplemental Video S5. Time is indicated in seconds after the first frame. Arrowheads point to lateral ingression of the fluorescent ForA construct. Bar, 10 μm. (B) Point scans of fluorescence intensities (I) at the site of an expanding wave or (II) at a retracting wave. The actin label is shown in red and the ForA in green. The noise in these curves is due to the microclustering of ForA. Times correspond to those of the image series in A.

Figure 3C and Supplemental Video S4 exemplify two cases in which one wave dominates another one. The dominating wave continues to propagate, expanding one inner territory on the expense of the other (56- and 70-s frames of Figure 3C). These cases confirm previous observations showing that refractoriness in the wave system is not always absolute (Gerhardt *et al.*, 2014), a finding that is relevant to the modeling of actin waves (Yochelis *et al.*, 2020).

Three formins are enriched in the external area

As shown in Figure 2, C–E, ForA, ForE, and ForH are similarly localized in actin wave patterns: these formins are preferentially recruited to the external area, which implies that they detach when the actin wave propagates into that area. To study this type of localization in detail, we focused on ForA.

The dynamics of ForA binding during wave propagation is illustrated in Figure 4. In the external area, ForA forms micropatches, which are highly dynamic as seen in Supplemental Video S5. When an actin wave is initiated in this area, ForA is locally dislodged, and the area of weak ForA decoration expands together with the propagation of a circular actin wave. The subsequent insertion of a retracting wave results in conversion of inner territory into the external area (Figure 4A, 167- and 195-s frames). The point scans I and II of Figure 4B illustrate the temporal relationship (I) between the passage of a leading wave and the decrease in ForA binding to the inner territory and (II) between a retracting wave and the increase in ForA binding to the external area.

ForA begins to occupy the external area from the side (arrowheads in the 167- and 195-s frames of Figure 4A, middle panel). Similar local entry from the free to the substrate-attached cell surface has previously been reported for PTEN, a 3-phosphatase that produces PI(4,5)P2 (Gerisch *et al.*, 2012). Accordingly, ForA is bound not only to the substrate-attached area (Figure 5A), but also to the free part of the cell surface (Figure 5B).

Membrane binding of ForA withstanding actin depolymerization

To prove that ForA binds to the plasma membrane without support of the cortical actin network, we incubated cells with 30 μM latrunculin A, a concentration sufficient to eliminate any actin filaments detectable by cryo-electron tomography (Heinrich *et al.*, 2014). GFP-ForA was bound under these conditions to the entire plasma membrane, including the membrane of pearls that formed when the supporting actin network was destroyed. Notably, no internal membranes were decorated by the ForA construct (Figure 5, C–E).

ForB associated with actin wave generation and propagation

ForB is most strongly enriched in actin waves, but is also weakly recruited to in the inner territory. The time series shown in Figure 6 exemplifies the association of GFP-ForBΔDAD with leading and trailing actin waves. The constitutively active ForB variant is already present during wave initiation (0-s frame) and is then further recruited to the expanding wave (144-s frame).

The insertion of the first wave in Figure 6, which is supposed to become a trailing wave, begins with indistinct and reversible

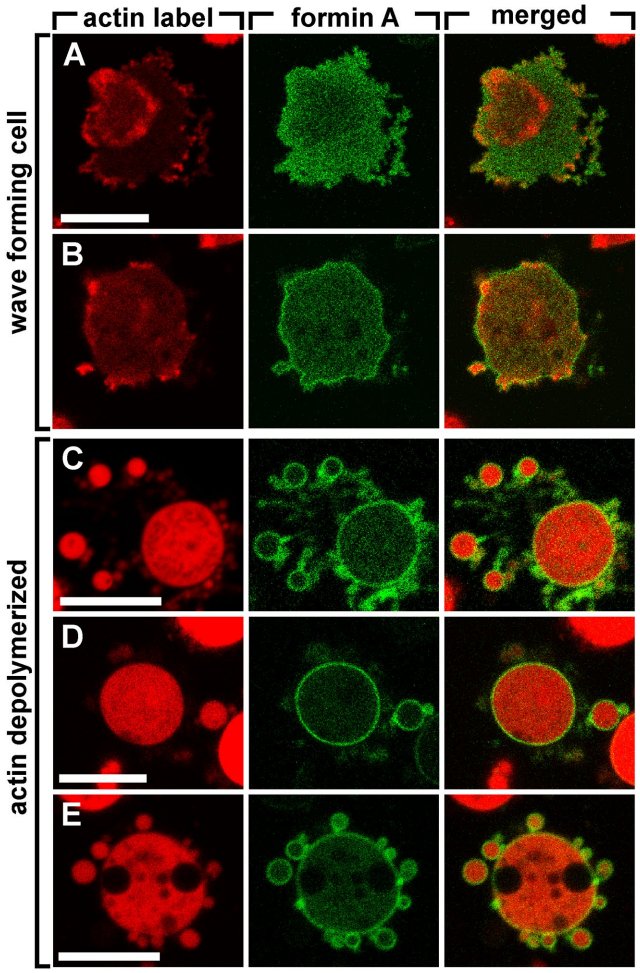

FIGURE 5: Membrane binding of ForA persists on depolymerization of the actin cortex. The cells expressed GFP-ForAΔDAD (green) and mRFP-LimEΔ (red). (A, B) A cell recovering from treatment with 5 μM latrunculin A shown at two confocal planes: (A) on the substrate-attached cell surface where an actin wave is formed and ForA is depleted in the inner territory; (B) in a cross-section through the cell at 1.2 μm beyond the substrate-attached surface where ForA is associated with the plasma membrane rather than enriched in actin clusters. (C–E) confocal cross-sections through cells incubated in 30 μM latrunculin A for various times: (C) 3 min; (D) 15 min; and (E) 20 min. With the highly concentrated blocker of actin polymerization, no remnants of polymerized actin are detectable using the LimEΔ label. The cells are rounded up under pearling of the plasma membrane. The ForA construct is bound to the entire plasma membrane including the pearls. Bars, 10 μm.

accumulations of ForB (234 s), before a continuous wave is formed (254 s). This wave is unusual in that it enlarges rather than reduces the size of the inner territory (286 and 298 s). Eventually, this wave is replaced by a typical trailing wave, which also begins with cloudy accumulations (334 s) before the distinct wave is formed (374 s). The entire time series from which the images of Figure 6 are taken is covered in Supplemental Video S6.

Coassembly of Formin B and Arp2/3 complex

The Arp2/3 complex acts in branching of actin filaments but not in their elongation (Chesarone and Goode, 2009; Block *et al.*, 2012). However, long branches separate the branch points from the substrate-attached plasma membrane within the actin waves (Jasnin *et al.*, 2019). It is therefore reasonable to assume that in building the architecture of actin waves, the Arp2/3 complex cooperates with the elongation factors present, such as ForB and VASP. A cooperation with VASP has recently been shown by Jasnin *et al.* (2019).

To explore an interrelation of ForB and Arp2/3 recruitment within the propagating waves, we made use of the fact that ForB is not uniformly distributed along the wave front, but is concentrated in patches. A patchy distribution in actin waves has previously been shown for the Arp2/3 complex (Jasnin *et al.*, 2019). Consequently, we explored whether ForB and Arp2/3 colocalize, using cells that coexpressed green fluorescent ForB and a red fluorescent subunit of the Arp2/3 complex (ArpD). As revealed by the scanning of fluorescence intensities parallel to the wave front (Figure 7, A–C), ForB and Arp2/3 coassembled into clusters; during wave propagation they were almost synchronously recruited to these clusters (Figure 7, D and E).

A transitory state of the pattern forming system characterized by ForB fluctuations

The state of the inner territory has a limited lifetime, returning to the state of the external area by insertion of a trailing wave (Gerhardt *et al.*, 2014). This transition is accompanied by fluctuations in ForB binding to the membrane. These ForB fluctuations preceding the insertion of a trailing wave are obvious in Supplemental Video S6.

Figure 8 illustrates the fluctuations of ForB at two points, which eventually became located to opposite sides of the boundary that separated inner territory from the external area (Figure 8A). At point I, ForB binding finally increased on integration into inner territory, while at point II, binding decreased to the low level of the external area (Figure 8, B and C). Remarkably, the actin label did not mirror the ForB fluctuations during the transitory state (Supplemental Video S7). The fluctuations of ForB are particularly apparent when the gain and loss of fluorescence intensity in consecutive frames of an image series is displayed, as shown in Supplemental Video S8.

Sensitivity of actin wave formation to formin inhibition

The presence of particular formins at specific sites of the wave pattern raised the question of whether wave formation and propagation depend on the activity of formins. Cultivating *Dictyostelium* cells on a perforated membrane revealed that at the sites of actin waves, the cells accumulated actin at the border of the holes in the grid and protruded into these holes (Jasnin *et al.*, 2016). This activity proved to be sensitive to SMIFH2, an inhibitor reported to compete with actin for the FH2 domain common to all formins (Rizvi *et al.*, 2009). In human cells, the specificity of SMIFH2 critically depends on the use of concentrations below 25 μM and incubation times of less than 1 h (Isogai *et al.*, 2015). In zebrafish embryos, the drug is cytotoxic even at 10 μM, but at 1 μM, no cytotoxicity has been observed (LeCorgne *et al.*, 2018).

Here we used a flow chamber to image wave formation while precisely controlling the concentration and application time of the inhibitor. At 1 μM, SMIFH2 reversibly abrogated wave formation (Figure 9A and Supplemental Video S9). The actin waves disappeared within 3 min of inhibitor addition and recovered within 5 min of removal of the inhibitor. Together with the actin waves, PIP3 disappeared from the inner territory. Remarkably, the cells did not round up in SMIFH2, as they did in latrunculin A, but still migrated with filamentous actin maintained at their front, and the bottom surface of the cells was populated with numerous actin puncta, most of them short lived.

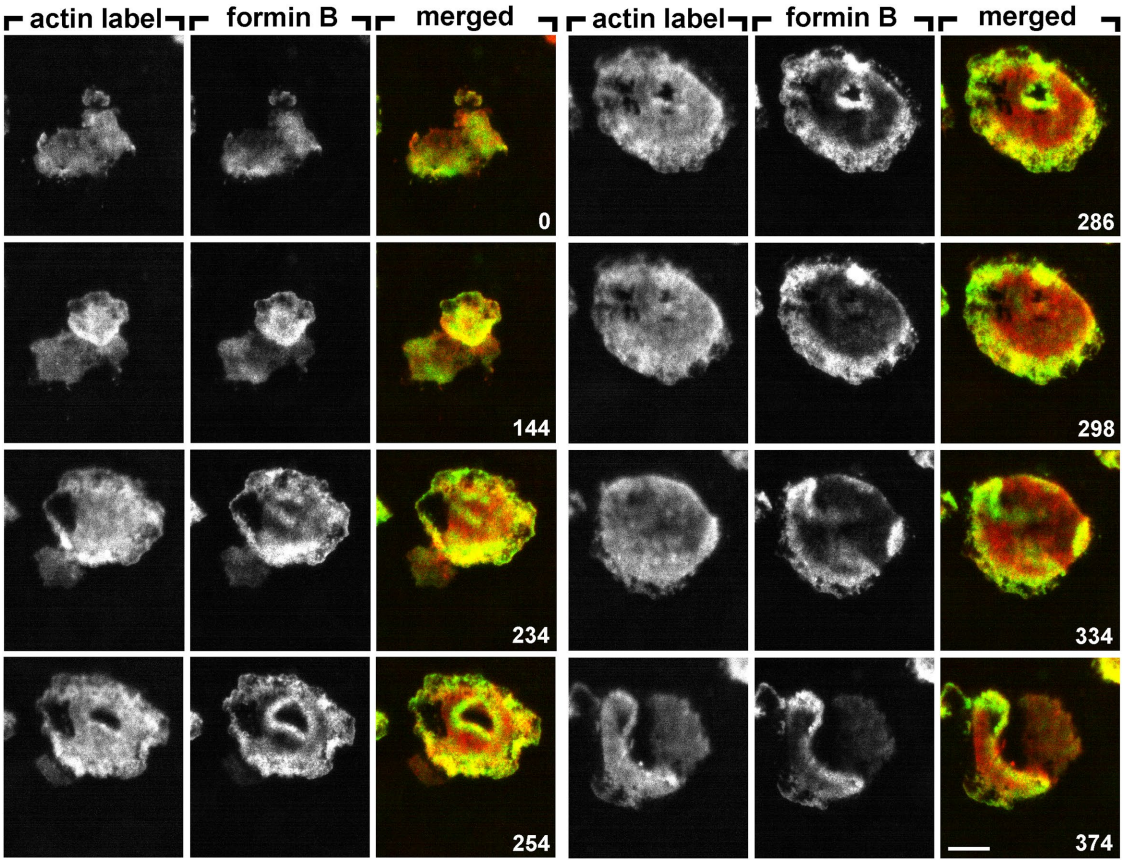

FIGURE 6: ForB localization to leading and trailing waves. The large cell shown in TIRF images expressed GFP-ForBΔDAD together with mRFP-LimEΔ. In the merged panels, the ForB construct is shown in green and the actin label in red. The time series show wave initiation and propagation (0- to 234-s frames) and the insertion of new waves. These waves divide the inner territory into a portion that remains inner territory and a portion that becomes outer area. The wave inserted first reverses direction, thus expanding the inner territory (254- to 298-s frames). The second inserted wave behaves as a typical trailing wave, propagating into the inner territory (334- and 374-s frames). Time is indicated in seconds. Bar, 10 μm. The full sequence is shown in Supplemental Video S6.

Since the short-lived puncta resembled the actin patches associated with clathrin-coated pits during their internalization (Heinrich *et al.*, 2008), we identified these structures using cells expressing both GFP-clathrin light chain and mRFP-LimEΔ. As previously reported for untreated cells (Heinrich *et al.*, 2008), the cells incubated with SMIFH2 showed mobile clathrin-coated pits, which diffused in the membrane for various times, became immobile when an actin patch was recruited and subsequently disappeared from the membrane (Figure 9B). Internalization in association with actin continued until the inhibitor was removed; this means for about 15 min of incubation with the inhibitor.

Actin patches other than the clathrin-associated puncta began to form after about 10 min of inhibitor addition. These patches expanded into larger plaques without affiliating with PIP3 (Figure 9, A and B). These data provide evidence for at least two actin-based activities that are less sensitive to SMIFH2 than the wave patterns, suggesting that formins are especially important for the wave forming system.

At the higher concentration of 10 μM SMIFH2, the cells dramatically changed shape. They extensively blebbed and extended long, cylindrical protrusions (Figure 9C and Supplemental Video S10). These changes were not reversible within 6 min of removal of the inhibitor. Nevertheless, the cells were still alive as evidenced by the discharge of the contractile vacuole, which continued to prevent the cells from swelling and thus from rounding up in the hypo-osmotic buffer solution.

DISCUSSION

Different sites of wave patterns are specified by distinct formins

Continuous turnover of filamentous actin at all sites of the wave pattern, the external area, the actin wave, and the inner territory, raised the question of which proteins are crucial for the nucleation and elongation of actin filaments at these different sites. Recent reconstruction of the actin architecture in wave patterns by cryo-electron tomography revealed assemblies of upright actin filaments branched by the Arp2/3 complex as a feature that distinguishes waves from the external area into which they propagate and also from the inner territory that they circumscribe (Jasnin *et al.*, 2019). Since in cell motility and endocytosis of *Dictyostelium* cells distinct formins differ in the sites of their activity and their function (Ramalingam *et al.*, 2015; Junemann *et al.*, 2016; Litschko *et al.*, 2019), these actin assembly factors have been candidates for organizing the actin wave pattern. In the present paper, we searched among VASP and six formins for polymerization factors that might be responsible for the differences in actin architecture (Figure 2). VASP and ForF were ubiquitously present in the wave patterns, whereas the other formins fell into three categories: ForB was preferentially recruited to the

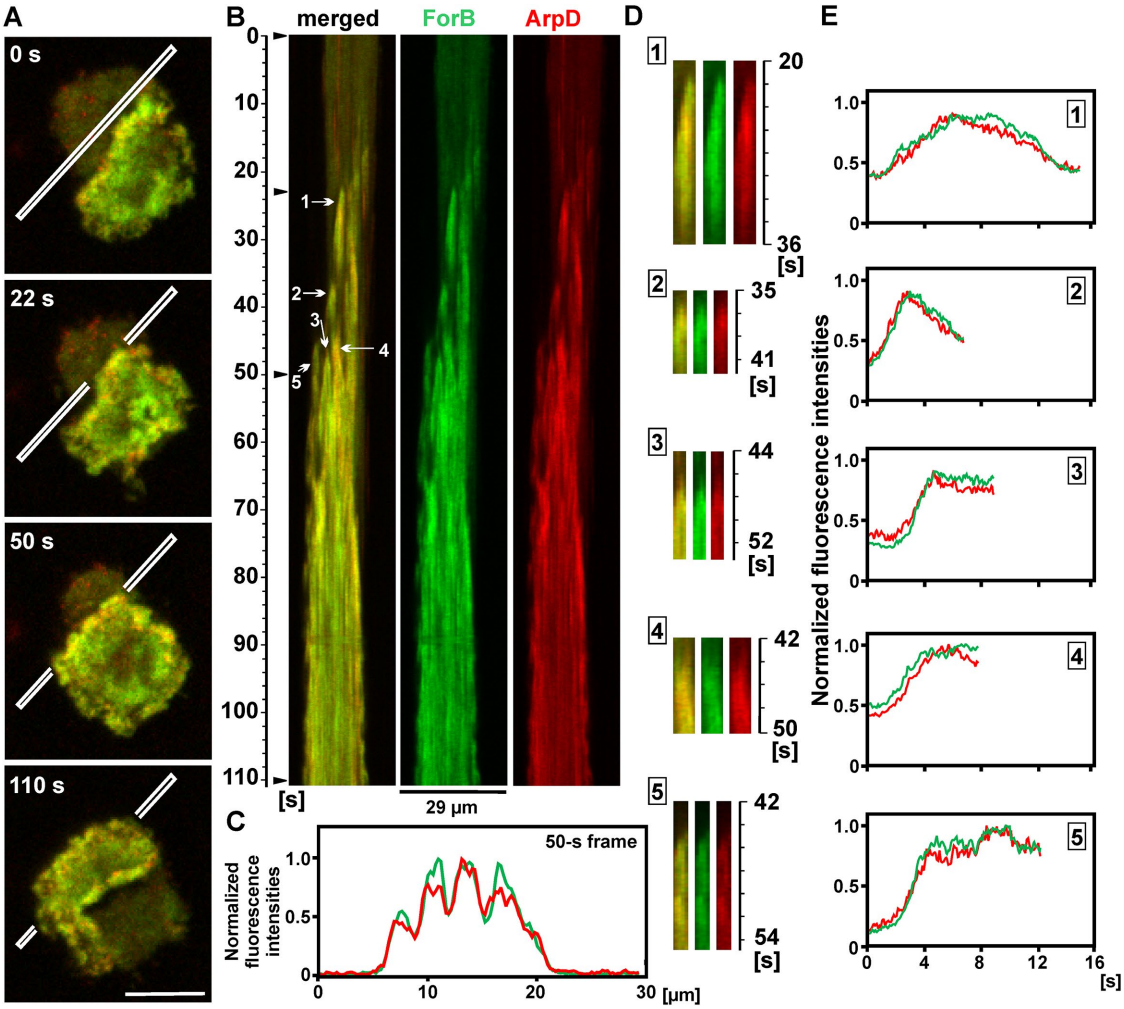

FIGURE 7: Colocalization of ForB and Arp2/3 clusters. The distribution of ForB and the Arp2/3 complex in a wave is scored in a cell expressing GFP-ForBΔDAD (green) and the mRFP-labeled Arp2/3 subunit ArpD (red). (A) TIRF images from a time series of wave propagation with the scan position for B and C indicated. (B) Kymograph presentation of ForB and ArpD fluorescence intensities along the scan indicated in A. Arrowheads on the left indicate times at which the images of A were taken. (C) Spatial distribution of fluorescence intensities parallel to the wave front along the scan in the 50-s image. (D) Single tracks of clusters from the kymograph, numbered as indicated in B. (E) Fluorescence intensities as a function of time, scanned along the corresponding tracks in D. Frame-to-frame interval 100 ms; bar in A, 10 µm.

propagating wave, ForG to the inner territory, and ForA, -E, and -H to the external area (Figures 2–4 and 6). These are the formins of interest in the context of pattern formation. The presence of formins in all regions of the pattern is consistent with the continuous turnover of the entire actin network (Figure 1), and the specific location of different formins is in accord with differences in the actin architecture among the external area, the wave, and the inner territory (Schroth-Diez *et al.*, 2009; Jasnin *et al.*, 2019).

A role of formins in establishing the pattern of actin waves is supported by extreme susceptibility of wave formation to the formin inhibitor SMIFH2. Incubation of cells with 1 µM of the inhibitor blocked wave formation (Figure 9A), although the cells accumulated F-actin at their front, were still motile, and endocytosed clathrin-coated vesicles (Figure 9B). Notably, not only actin wave formation is sensitive to the inhibitor but also PIP3 synthesis in the inner territory. This effect relates to the question of whether the recruitment of PI3-kinase to the membrane depends on actin, as proposed by Sasaki *et al.* (2007). The role of actin needs to be specified, since on one hand, Fukushima *et al.* (2019), using a moderate concentration of 5 µM latrunculin A, found that a functional cytoskeleton is not required, and on the other hand, Gerisch *et al.* (2019) reported that efficient blockage of actin polymerization by a combination of lactrunculin A and cytochalasin A inhibits the synthesis of PIP3. The data presented here suggest that specifically formin-mediated actin polymerization plays a role in the activation of PI3-kinase.

An N-terminal ForG construct reveals dynamics of the inner territory

ForG localizes to the base of a phagocytic or macropinocytic cup and drives elongation of filaments nucleated by the Arp2/3 complex to facilitate cup closure (Junemann *et al.*, 2016). The accumulation of ForG in the inner territory of a wave pattern (Figures 2B and 3) is in accord with the notion that this pattern resembles a frustrated phagocytic cup, with the actin wave corresponding to the border of the cup and the inner territory to its bottom (Gerisch *et al.*, 2009). With its GTPase-binding domain, ForG recognizes activated RasB

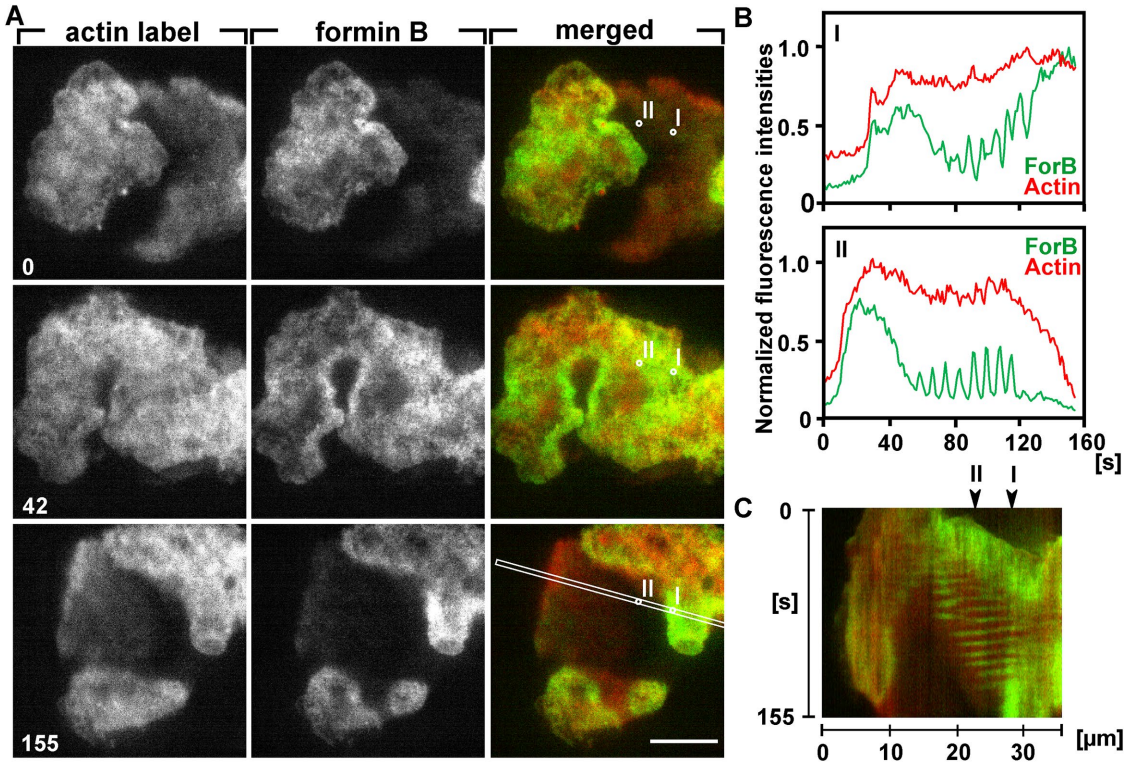

FIGURE 8: ForB fluctuations during a transition state in pattern dynamics. (A) Three stages of wave pattern in a large cell expressing mRFP-LimEΔ as a label for filamentous actin (red), and GFP-ForBΔDAD (green in the merged images). In these TIRF images, time is indicated in seconds after the first frame. Bar, 10 µm. The entire sequence is shown in Supplemental Video S7. (B) Scans of fluorescence intensities of the actin label (red) and the ForB construct (green) at points I and II as indicated in the merged images of A. After a period of fluctuations, point I became integrated into the wave and inner territory while point II became, again after a period of fluctuations, incorporated into the external area. The two events were synchronously recorded within the same large cell. Fluorescence intensities in both panels were normalized by setting the highest fluorescence intensities in the top panel to 1. (C) Kymograph of pattern dynamics along the line indicated in the merged image on the bottom of A. In the kymograph, ForB fluctuations appear as periodic stripes.

and -G (Junemann *et al.*, 2016). Consistently, Ras is activated in the inner territory to which ForG is recruited (Sasaki *et al.*, 2007; Ecke and Gerisch, 2017; Fukushima *et al.*, 2019; Gerisch *et al.*, 2019).

Large cells produced by electric pulse–induced fusion enabled multiple inner territories to coexist. Using a ForG label for these territories, we studied their dynamics on wave propagation and collision. Figure 3B and Supplemental Video S3 exemplify the fusion of inner territories when colliding waves extinguish each other, which is a feature of an excitable system. In addition to these typical cases, incidents of collision have been observed with one wave overriding the other, thus continuing to propagate. The examples presented in Figure 3C and Supplemental Video S4 show the area in front of the wave losing its ForG-N decoration while the area behind the wave is expanding.

ForA enriched in the external area coincides with PI(4,5)P2

In a polarized migrating cell, ForA localizes to the actin cortex at the contractile rear and participates in its retraction (Ramalingam *et al.*, 2015). Accordingly, in wave patterns ForA is coenriched with filamentous myosin II in the external area, which tends to contract (Schroth-Diez *et al.*, 2009). Our finding that ForA still binds to the membrane when actin is efficiently depolymerized (Figure 5, C–E) is consistent with a previous report that ForA does bind to PI(4,5)P2 (Ramalingam *et al.*, 2015). Moreover, the reduced recruitment of ForA to the inner territory (Figures 2C and 4) parallels the lower PI(4,5)P2 content of this territory relative to the external area (Gerisch *et al.*, 2011).

ForB fluctuations uncover transitory states of pattern formation

Peculiar to ForB are the fluctuations of its binding to the cytoplasmic face of the plasma membrane during a transitory state of actin wave formation (Supplemental Videos S6–S8). During this state a decision is made on whether a point in the field will be integrated into inner territory or the external area, as illustrated in Figure 8. Thus, the fluctuating ForB binding unveils states in the generation of a cellular pattern, in which two domains of the plasma membrane in connection with the actin cortex become sharply separated, notably without the establishment of a diffusion barrier between them.

MATERIALS AND METHODS

Cell culture and sample preparation for light microscopy

Cells of *D. discoideum* strain AX2-214 expressing fluorescent proteins were cultivated in Petri dishes containing nutrient medium (Malchow *et al.*, 1972) supplemented with 10 µg/ml Blasticidin S (Life Technologies, Grand Island, NY) and/or 10 µg/ml Geneticin (Sigma-Aldrich, St. Louis, MO). Cells were harvested before confluency. Temperature throughout culture and experiments was 21 ± 2°C.

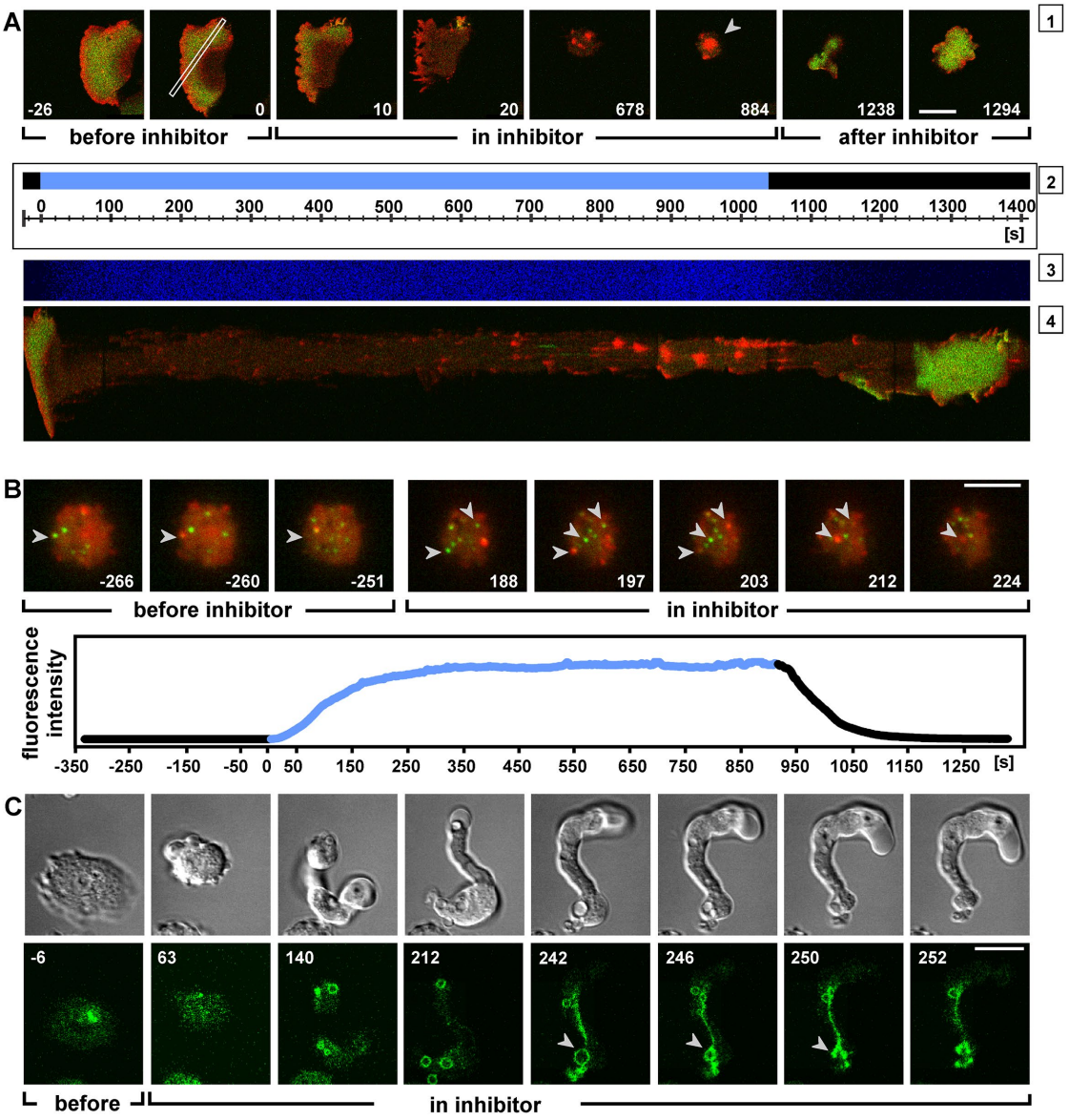

FIGURE 9: High sensitivity of wave formation to the formin inhibitor SMIFH2. Cells were exposed in a flow chamber to a constant flow of the inhibitor. The solutions were supplemented with CY5 as a fluorescent indicator of the temporal concentration changes during addition and removal of the inhibitor. Scale bars in the images, 10 μm. (A) A cell expressing GFP-PHcrac as a label for PIP3 (green) and mRFP-LimEΔ for F-actin (red) exposed to 1 μM SMIFH2. The four panels show from top to bottom the following: (1) Confocal images of the PIP3 and actin labels in the cell transiently exposed to the inhibitor. The arrowhead in the 884-s image points to a large actin patch that resisted inhibitor action. Time is indicated in seconds before and after arrival of the inhibitor. The same sequence is shown in Supplemental Video S9. (2) Period from addition to removal of the inhibitor (blue) and time scale for all panels in A. (3) Recording of fluorescence intensities of the marker CY5 (blue). (4) Kymogram of fluorescence intensities along the line-scan indicated in the zero-time image of panel 1. (B) A cell expressing GFP-clathrin light chain (green) and mRFP-LimEΔ for F-actin (red) exposed again to 1 μM of the inhibitor. The images on the top show clathrin-coated pits shifting from green to red label (arrowheads) before they disappear from the TIRF-illuminated region close to the membrane. The curve on the bottom shows the temporal profile of the CY5 fluorescence intensity as an indicator of inhibitor concentrations. The period from arrival to removal of the inhibitor is shown in blue. (C) A cell expressing GFP-dajumin to visualize the contractile vacuole system and mRFP-LimEΔ (the latter is shown only in Supplemental Video S10). Time is indicated in seconds before and after the supply of 10 μM SMIFH2. Top panels show DIC images of altered cell shape and bottom panels the corresponding confocal fluorescence images. Arrowheads point to the discharge of a large vacuole (in the first images vacuoles are out of focus). The same sequence is shown in Supplemental Video S10.

Large cells were produced by electric pulse–induced fusion (Gerisch *et al.*, 2013). Cells were washed twice in 17 mM K/Na-phosphate buffer, pH 6.0 (PB), adjusted to 1.5×10^7 cells/ml, and gently shaken in the buffer for 3 h in roller tubes, allowing the cells to agglutinate. Aliquots of the suspension were gently transferred to electroporation cuvettes with an electrode distance of 4 mm and fused in a Bio-Rad Gene Pulser Model 1652077 (Bio-Rad Laboratories, Hercules, CA) by applying three pulses of 1 kV and 1 or 3 μF at

1-s intervals. After 5 min, 50 µl of the fused-cell suspension was added to 3 ml of PB supplemented with 2 mM $CaCl_2$ and 2 mM $MgCl_2$ in an HCl-cleaned cover-glass bottom dish (FluoroDish; WPI, Sarasota, FL) for TIRF or confocal imaging.

Cell strains

Cells shown in Figure 1A expressed superfolder (sf) GFP-PHcrac (Müller-Taubenberger and Ishikawa-Ankerhold, 2013) in combination with mRFP-LimEΔ (Fischer *et al.*, 2004). In Figure 1C, GFP-filamin (full length) (Khaire *et al.*, 2007); in Figure 2A, GFP-VASP (full length) (Schirenbeck *et al.*, 2006); in Figures 2B and 3, cells expressing YFP-ForG-N (1–423) (Junemann *et al.*, 2016); in Figures 2C, 4, and 5, GFP-ForAΔDAD in ForA-null cells (Ramalingam *et al.*, 2015); in Figure 2D, GFP-ForE-N (Ramalingam, 2009); in Figure 2E, GFP-ForHΔDAD (Winterhoff *et al.*, 2014) in combination with mRFP-LimEΔ; and in Figures 2F and 6–8, GFP-ForBΔDAD in combination with mRFP-LimEΔ or mRFP-ArpD (Insall *et al.*, 2001) were used.

For the flow chamber experiments of Figure 9, cells expressing mRFP-LimEΔ as a label for F-actin, in combination with either sf GFP-PHcrac for PIP3 (Figure 9A), clathrin light-chain-GFP (Wang *et al.*, 2006) for clathrin-coated pits (Figure 9B), or GFP-dajumin (Gabriel *et al.*, 1999) for the contractile vacuole network (Figure 9C), were used.

Image acquisition and data analysis

TIRF images of the substrate-attached membrane region were acquired at a GE DeltaVision Elite system (GE Healthcare Bio-Sciences, Marlborough, MA) based on an OLYMPUS IX-71 inverted microscope, with an Olympus TIRF 100×/1.49 UAPON objective and a PCO sCMOS 5.5 camera. For imaging the cells at high frequency in TIRF mode (Figure 7), a Zeiss Elyra PS.1 microscope (Carl Zeiss Microscopy, Jena, Germany) with an alpha Plan-Apochromat 63×/1,46 Oil Corr TIRF objective and two PCO pco. edge 4.2 m sCMOS cameras (PCO-Tech, Romulus, MI) was used. For confocal recordings, a Zeiss LSM 780 microscope equipped with a Plan-Apo 63×/NA 1.46 oil immersion objective was used.

Images were analyzed using the image-processing package Fiji (http://Fiji.sc/Fiji) developed by Schindelin *et al.* (2012) on the basis of ImageJ (http://imagej.nih.gov/ij). Line-scans and point-scans were performed using Fiji. To plot the charts, data were imported in Microsoft Excel sheets.

Images in Figure 1C and Supplemental Video S1 were processed through SRRFs with the plug-in NanoJ-SRRF, a part of the open-source superresolution microscopy image analysis toolbox NanoJ designed by Laine *et al.* (2019). The images were acquired at a frame rate of 1/s with an exposure time of 100 ms. Each single image was processed using the following settings for the SRRF algorithm: radiality magnification 5, ring radius 3, axes 6.

Photoconversion of Eos-actin

To study actin dynamics in the inner territory (Figure 1B), we used the photoconvertible fluorescent protein Eos as a tag (Wiedenmann *et al.*, 2004). For the generation of a pDEX-DdEos expression vector, the sequence of monomeric Eos (Wiedenmann *et al.*, 2004) was adapted to the codon usage of *D. discoideum* and cloned into pDEX (bsr), enabling expression under control of an actin-15 promoter (Müller-Taubenberger, 2006). The full-length coding sequence of act16 (DDB_G0272248), one of 17 identical actin proteins encoded in *D. discoideum*, was cloned in frame into the *Eco*RI site of the pDEX-DdEos vector. The sequences of DdEos and actin 16 were separated by a linker sequence, GSGTAGPGSTGSGTEF. DdEos-actin cells were cultivated in the presence of 10 µg/ml Blasticidin S.

For photoconversion, a 405-nm diode laser, 100 mW, was used on the GE DeltaVision Elite system. The laser was focused onto the actin cortex of the substrate-attached cell surface and a flash with an exposure time of 80 or 250 ms was applied. The cells were imaged in the TIRF mode using 488/525 nm for excitation/emission of the green version of Eos, and 568/584 nm of the photoconverted red version. Local fluorescence intensities were measured with point-scans of 36 × 36 pixels using a plug-in of Fiji-ImageJ.

Treatment with latrunculin A

Cells expressing mRFP-LimEΔ in combination with GFP-ForAΔDAD in ForA-null background were allowed to settle on a glass bottom dish (FluoroDish; WPI, Sarasota, FL), washed with PB, and treated after 1 h starvation with 30 µM latrunculin A (Life Technologies, Molecular Probes, Grand Island, NY) and imaged in confocal mode.

Treatment with SMIFH2

For flow chamber experiments, cells in PB were allowed to settle on the glass bottom of a six-channel µ-slide IV 0.5 (IBIDI GmbH, Munich, Germany), which has an O_2-permeable cover sheet. A stock solution of 10 mM SMIFH2 (Sigma-Aldrich, St. Louis, MO) in dimethyl sulfoxide was freshly diluted to 1 or 10 µM in PB and supplemented with 10 µM sulfo-cyanine-5-carboxylic acid (CY5) (Lumiprobe, Hunt Valley, MD) to record arrival and depletion of the inhibitor solution by excitation at 633 nm and emission at 679 nm. Cells were exposed to a continuous flow of 0.25 ml/min of PB for at least 4 min before the inhibitor application. The solutions were pumped through the µ-slide at the same speed using a Harvard PHD 200 pump set (Harvard Apparatus, Holliston, MA) on the lee side as described by Etzrodt *et al.* (2006).

ACKNOWLEDGMENTS

We thank Martin Spitaler and his team at the Imaging Facility of the Max Planck Institute of Biochemistry for cooperation and Petra Fey and dictyBase for providing information. This work was funded by the Max Planck Society to G.G. and by a grant of the Deutsche Forschungsgemeinschaft to J.F. (FA330/13-1).

REFERENCES

Alberts AS (2001). Identification of a carboxyl-terminal diaphanous-related formin homology protein autoregulatory domain. J Biol Chem 276, 2824–2830.

Block J, Breitsprecher D, Kühn S, Winterhoff M, Kage F, Geffers R, Duwe P, Rohn JL, Baum B, Brakebusch C, *et al.* (2012). FMNL2 drives actin-based protrusion and migration downstream of cdc42. Curr Biol 22, 1005–1012.

Breitsprecher D, Kiesewetter AK, Linkner J, Urbanke C, Resch GP, Small JV, Faix J (2008). Clustering of VASP actively drives processive, WH2 domain-mediated actin filament elongation. EMBO J 27, 2943–2954.

Bretschneider T, Anderson K, Ecke M, Müller-Taubenberger A, Schroth-Diez B, Ishikawa-Ankerhold HC, Gerisch G (2009). The three-dimensional dynamics of actin waves, a model of cytoskeletal self-organization. Biophys J 96, 2888–2900.

Bretschneider T, Diez S, Anderson K, Heuser J, Clarke M, Müller-Taubenberger A, Köhler J, Gerisch G (2004). Dynamic actin patterns and Arp2/3 assembly at the substrate-attached surface of motile cells. Curr Biol 14, 1–10.

Chesarone MA, Goode BL (2009). Actin nucleation and elongation factors: mechanisms and interplay. Curr Opin Cell Biol 21, 28–37.

Culley S, Tosheva KL, Matos Pereira P, Henriques R (2018). SRRF: universal live-cell super-resolution microscopy. Int J Biochem Cell Biol 101, 74–79.

Diez S, Gerisch G, Anderson K, Müller-Taubenberger A, Bretschneider T (2005). Subsecond reorganization of the actin network in cell motility and chemotaxis. Proc Natl Acad Sci USA 102, 7601–7606.

Ecke M, Gerisch G (2017). Co-existence of Ras activation in a chemotactic signal transduction pathway and in an autonomous wave-forming system. Small GTPases 10, 72–80.

Etzrodt M, Ishikawa HC, Dalous J, Müller-Taubenberger A, Bretschneider T, Gerisch G (2006). Time-resolved responses to chemoattractant, characteristic of the front and tail of Dictyostelium cells. FEBS Lett 580, 6707–6713.
Fischer M, Haase I, Simmeth E, Gerisch G, Müller-Taubenberger A (2004). A brilliant monomeric red fluorescent protein to visualize cytoskeleton dynamics in Dictyostelium. FEBS Lett 577, 227–232.
Fukushima S, Matsuoka S, Ueda M (2019). Excitable dynamics of Ras triggers spontaneous symmetry breaking of PIP3 signaling in motile cells. J Cell Sci 132, jcs224121.
Gabriel D, Hacker U, Köhler J, Müller-Taubenberger A, Schwartz JM, Westphal M, Gerisch G (1999). The contractile vacuole network of Dictyostelium as a distinct organelle: its dynamics visualized by a GFP marker protein. J Cell Sci 112, 3995–4005.
Gerhardt M, Ecke M, Walz M, Stengl A, Beta C, Gerisch G (2014). Actin and PIP3 waves in giant cells reveal the inherent length scale of an excited state. J Cell Sci 127, 4507–4517.
Gerisch G, Ecke M, Neujahr R, Prassler J, Stengl A, Hoffmann M, Schwarz US, Neumann E (2013). Membrane and actin reorganization in electropulse-induced cell fusion. J Cell Sci 126, 2069–2078.
Gerisch G, Ecke M, Schroth-Diez B, Gerwig S, Engel U, Maddera L, Clarke M (2009). Self-organizing actin waves as planar phagocytic cup structures. Cell Adh Migr 3, 373–382.
Gerisch G, Ecke M, Wischnewski D, Schroth-Diez B (2011). Different modes of state transitions determine pattern in the phosphatidylinositide-actin system. BMC Cell Biol 12, 42.
Gerisch G, Prassler J, Butterfield N, Ecke M (2019). Actin waves and dynamic patterning of the plasma membrane. Yale J Biol Med 92, 397–411.
Gerisch G, Schroth-Diez B, Müller-Taubenberger A, Ecke M (2012). PIP3 waves and PTEN dynamics in the emergence of cell polarity. Biophys J 103, 1170–1178.
Goode BL, Eck MJ (2007). Mechanism and function of formins in the control of actin assembly. Annu Rev Biochem 76, 593–627.
Gustafsson N, Culley S, Ashdown G, Owen DM, Pereira PM, Henriques R (2016). Fast live-cell conventional fluorophore nanoscopy with ImageJ through super-resolution radial fluctuations. Nat Commun 7, 12471.
Han Y-H, Chung CY, Wessels D, Stephens S, Titus MA, Soll DR, Firtel RA (2002). Requirement of a vasodilator-stimulated phosphoprotein family member for cell adhesion, the formation of filopodia, and chemotaxis in Dictyostelium. J Biol Chem 277, 49877–49887.
Heinrich D, Ecke M, Jasnin M, Engel U, Gerisch G (2014). Reversible membrane pearling in live cells upon destruction of the actin cortex. Biophys J 106, 1079–1091.
Heinrich D, Youssef S, Schroth-Diez B, Engel U, Aydin D, Blummel J, Spatz JP, Gerisch G (2008). Actin-cytoskeleton dynamics in non-monotonic cell spreading. Cell Adh Migr 2, 58–68.
Insall R, Müller-Taubenberger A, Machesky L, Köhler J, Simmeth E, Atkinson SJ, Weber I, Gerisch G (2001). Dynamics of the Dictyostelium Arp2/3 complex in endocytosis, cytokinesis, and chemotaxis. Cell Motil Cytoskeleton 50, 115–128.
Isogai T, van der Kammen R, Innocenti M (2015). SMIFH2 has effects on formins and p53 that perturb the cell cytoskeleton. Sci Rep 5, 9802.
Jasnin M, Beck F, Ecke M, Fukuda Y, Martinez-Sanchez A, Baumeister W, Gerisch G (2019). The architecture of traveling actin waves revealed by cryo-electron tomography. Structure 27, 1211–1223.
Jasnin M, Ecke M, Baumeister W, Gerisch G (2016). Actin organization in cells responding to a perforated surface, revealed by live imaging and cryo-electron tomography. Structure 24, 1031–1043.
Junemann A, FilićV, Winterhoff M, Nordholz B, Litschko C, Schwellenbach H, Stephan T, Weber I, Faix J (2016). A Diaphanous-related formin links Ras signaling directly to actin assembly in macropinocytosis and phagocytosis. Proc Natl Acad Sci USA 113, 7464–7473.
Khaire N, Müller R, Blau-Wasser R, Eichinger L, Schleicher M, Rief M, Holak TA, Noegel AA (2007). Filamin-regulated F-actin assembly is essential for morphogenesis and controls phototaxis in Dictyostelium. J Biol Chem 282, 1948–1955.
Kitayama C, Uyeda TQP (2003). ForC, a novel type of formin family protein lacking an FH1 domain, is involved in multicellular development in Dictyostelium discoideum. J Cell Sci 116, 711–723.
Laine RF, Tosheva KL, Gustafsson N, Gray RDM, Almada P, Albrecht D, Risa GT, Hurtig F, Lindås A-C, Baum B, *et al*. (2019). NanoJ: a high-performance open-source super-resolution microscopy toolbox. J Phys D Appl Phys 52, 163001.
Lammers M, Rose R, Scrima A, Wittinghofer A (2005). The regulation of mDia1 by autoinhibition and its release by Rho*GTP. EMBO J 24, 4176–4187.
LeCorgne H, Tudosie AM, Lavik K, Su R, Becker KN, Moore S, Walia Y, Wisner A, Koehler D, Alberts AS, *et al*. (2018). Differential toxicity of mDia formin-directed functional agonists and antagonists in developing Zebrafish. Front Pharmacol 9, 340–350.
Li F, Higgs HN (2005). Dissecting requirements for auto-inhibition of actin nucleation by the formin, mDia1. J Biol Chem 280, 6986–6992.
Litschko C, Brühmann S, Csiszár A, Stephan T, Dimchev V, Damiano-Guercio J, Junemann A, Körber S, Winterhoff M, Nordholz B, *et al*. (2019). Functional integrity of the contractile actin cortex is safeguarded by multiple Diaphanous-related formins. Proc Natl Acad Sci USA 116, 3594–3603.
Malchow D, Nägele B, Schwarz H, Gerisch G (1972). Membrane-bound cyclic AMP phosphodiesterase in chemotactically responding cells of Dictyostelium discoideum. Eur J Biochem 28, 136–142.
Müller-Taubenberger A (2006). Application of fluorescent protein tags as reporters in live-cell imaging studies. Methods Mol Biol 346, 229–246.
Müller-Taubenberger A, Ishikawa-Ankerhold HC (2013). Fluorescent reporters and methods to analyze fluorescent signals. Methods Mol Biol 983, 93–112.
Nezami AG, Poy F, Eck MJ (2006). Structure of the autoinhibitory switch in formin mDia1. Structure 14, 257–263.
Ramalingam N (2009). Diaphanous-related formins: characterization of mouse mDia1, and ForA/dDia3 from Dictyostelium discoideum amoebae. Doctoral dissertation, LMU Munich.
Ramalingam N, Franke C, Jaschinski E, Winterhoff M, Lu Y, Brühmann S, Junemann A, Meier H, Noegel AA, Weber I, *et al*. (2015). A resilient formin-derived cortical actin meshwork in the rear drives actomyosin-based motility in 2D confinement. Nat Commun 6, 8496–8510.
Ramalingam N, Zhao H, Breitsprecher D, Lappalainen P, Faix J, Schleicher M (2010). Phospholipids regulate localization and activity of mDia1 formin. Eur J Cell Biol 89, 723–732.
Rivero F, Muramoto T, Meyer A-K, Urushihara H, Uyeda TQP, Kitayama C (2005). A comparative sequence analysis reveals a common GBD/FH3-FH1-FH2-DAD architecture in formins from Dictyostelium, fungi and metazoa. BMC Genomics 6, 28–44.
Rizvi SA, Neidt EM, Cui J, Feiger Z, Skau CT, Gardel ML, Kozmin SA, Kovar DR (2009). Identification and characterization of a small molecule inhibitor of formin-mediated actin assembly. Chem Biol 16, 1158–1168.
Sasaki AT, Janetopoulos C, Lee S, Charest PG, Takeda K, Sundheimer LW, Meili R, Devreotes PN, Firtel RA (2007). G protein-independent Ras/PI3K/F-actin circuit regulates basic cell motility. J Cell Biol 178, 185–191.
Schindelin J, Arganda-Carreras I, Frise E, Kaynig V, Longair M, Pietzsch T, Preibisch S, Rueden C, Saalfeld S, Schmid B (2012). Fiji: an open-source platform for biological-image analysis. Nat Methods 9, 676–682.
Schirenbeck A, Arasada R, Bretschneider T, Stradal TE, Schleicher M, Faix J (2006). The bundling activity of vasodilator-stimulated phosphoprotein is required for filopodium formation. Proc Natl Acad Sci USA 103, 7694–7699.
Schirenbeck A, Bretschneider T, Arasada R, Schleicher M, Faix J (2005). The Diaphanous-related formin dDia2 is required for the formation and maintenance of filopodia. Nat Cell Biol 7, 619–625.
Schroth-Diez B, Gerwig S, Ecke M, Hegerl R, Diez S, Gerisch G (2009). Propagating waves separate two states of actin organization in living cells. HFSP J 3, 412–427.
Seth A, Otomo C, Rosen MK (2006). Autoinhibition regulates cellular localization and actin assembly activity of the diaphanous-related formins FRLalpha and mDia1. J Cell Biol 174, 701–713.
Wang J, Wang Y, O'Halloran TJ (2006). Clathrin light chain: Importance of the conserved carboxy terminal domain to function in living cells. Traffic 7, 824–832.
Watanabe N, Kato T, Fujita A, Ishizaki T, Narumiya S (1999). Cooperation between mDia1 and ROCK in Rho-induced actin reorganization. Nat Cell Biol 1, 136–143.
Wiedenmann J, Ivanchenko S, Oswald F, Schmitt F, Röcker C, Salih A, Spindler K-D, Nienhaus GU (2004). EosFP, a fluorescent marker protein with UV-inducible green-to-red fluorescence conversion. Proc Natl Acad Sci USA 101, 15905–15910.
Winterhoff M, Junemann A, Nordholz B, Linkner J, Schleicher M, Faix J (2014). The Diaphanous-related formin dDia1 is required for highly directional phototaxis and formation of properly sized fruiting bodies in Dictyostelium. Eur J Cell Biol 93, 212–224.
Yochelis A, Beta C, Gov N (2020). Excitable solitons: annihilation, crossover, and nucleation of pulses in mass-conserving activator-inhibitor media. doi:arXiv:1907.10264v3.